# Melting of multilayer colloidal crystals confined between two walls

Y. Peng (□□), Z.-R. Wang (□□□), A. M. Alsayed, A. G. Yodh, and Y. Han (□□□)

Phys. Rev. E **83**, 011404 — Published 25 January 2011

DOI: 10.1103/PhysRevE.83.011404

# Melting of Multilayer Colloidal Crystals Confined Between Two Walls

Y. Peng[1] (彭毅), Z.-R. Wang[1] (王梓任), A. M. Alsayed[2,3], A. G. Yodh[2] and Y. Han[1,*] (韩一龙)
[1] *Department of Physics, Hong Kong University of Science and Technology, Clear Water Bay, Hong Kong, China**
[2] *Department of Physics and Astronomy, University of Pennsylvania 209 South 33rd St., Philadelphia, PA 19104 USA and*
[3] *Complex Assemblies of Soft Matter, CNRS/UPENN/Rhodia UMI 3254, Bristol, PA 19007, USA*

Video microscopy is employed to study the melting behaviors of multilayer colloidal crystals composed of diameter-tunable microgel spheres confined between two walls. We systematically explore film thickness effects on the melting process and on the phase behaviors of single crystal and polycrystalline films. Thick films ($> 4$ layers) are observed to melt heterogeneously, while thin films ($\leq 4$ layers) melt homogeneously, even for polycrystalline films. Grain-boundary melting dominates other types of melting processes in polycrystalline films thicker than 12-layers. A new effect is discovered in films between 5- and 12-layers: heterogeneous melting from dislocations is found to coexist with grain-boundary melting. In dislocation melting, liquid nucleates at dislocations and forms lake-like domains embedded in the larger crystalline matrix; the "lakes" are observed to diffuse, interact, merge with each other, and eventually merge with large strips of liquid melted from grain boundaries. Thin film melting is qualitatively different: thin films homogeneously melt by generating many small defects which need not nucleate at grain boundaries or dislocations. For 3- and 4-layer thin films, different layers are observed to have the same melting point, but surface layers melt faster than bulk layers. Within our resolution, 2- to 4-layer films appear to melt in one step, while monolayers melt in two steps with an intermediate hexatic phase.



## I. INTRODUCTION

Crystal melting has been studied for more than 100 years, but many questions about melting mechanisms remain to be answered [1]. Dimensionality, for example, plays an important role in melting; three-dimensional (3D) crystals directly melt into a liquid phase via a first order transition, but the nature of two-dimensional (2D) crystal melting has been richly debated for decades [2]. In the popular Kosterlitz-Thouless-Halperin-Nelson-Young (KTHNY) scenario [3, 4], 2D crystals first melt into a hexatic phase and then melt from the hexatic phase to a liquid phase via two continuous phase transitions associated with the creation of dislocations and disclinations, respectively. Since 3D and 2D melting are so qualitatively different, it is natural to wonder about the melting behavior of thin films. Do hexatic-like phases exist in thin films? Do critical thicknesses exist wherein melting behavior changes qualitatively? How do grain boundaries and other defects affect thin film melting, and where does melting start in single crystal films without grain boundaries? We began exploring some of these questions in a recent paper [5], and in this contribution we describe further experimentation that supports claims of ref. [5] and introduces some new melting mechanisms.

Experimental investigation of thin-film melting is challenging. To date, a few atomic and molecular systems have been experimentally studied [6, 7] wherein a molecular thin film is placed with one side on a solid substrate and the other side in contact with vapor. Consequently, melting starts from the film-vapor interface and progresses through the film. Heterogeneous melting from grain boundaries, film-wall interfaces and other defects have not be studied [1], because they are overwhelmed by the surface melting mechanism. Moreover, molecular thin-film melting experiments rarely provide microscopic details with single-particle resolution.

Here we are concerned with where melting starts and how the liquid phase nucleates and grows in thin films. Generally, crystals are believed to melt *heterogeneously* via [1]: (1) *surface melting* from the interface between crystal and vapor; (2) *interfacial melting* from the interface between crystal and a solid substrate made of a different material, and (3) *grain-boundary melting* from the interface between two crystalline domains of the same substance. In this paper we also show melting from dislocations in thin films of intermediate thickness (5- to 12-layers). In all of these melting processes, liquids nucleate and then grow into the bulk. Usually one class of heterogeneous melting dominates and suppresses other types of heterogeneous melting, even when samples are rapidly heated.

Although heterogeneous melting is most often encountered in experiment, most theoretical and simulation studies focus on *homogenous melting*. In *homogenous melting*, surface effects are assumed to be small and liquid nucleates in the interior of a uniformly superheated substance without preferential sites. In practice, however, all materials have surfaces and/or interfaces; moreover, in 3D, preemptive heterogeneous melting is generally found to dominate homogenous melting, even when samples are rapidly heated. Thin film solids are different from their fully 3D analogues, offering experimenters a rich variety of interfaces, grain boundaries and other defects which can affect melting. Thus, these media present us with opportunities to explore many fundamental questions, which, potentially have technological implications as well.

This paper investigates the melting behaviors of thin films composed of colloidal particles. Colloids are outstanding systems for melting studies because the trajectories of individual particles are measurable by video microscopy. Melting of 2D colloidal crystals has been well investigated [8–12], but melting of a 3D and/or multilayer crystals with conventional colloidal particles has proven much more difficult to study. For example, magnetic spheres can form crystals in 2D confinement and their dipolar repulsions can be tuned by the magnetic field [11], but in 3D they often aggregate. In a different vein, colloidal crystallization has been studied (e.g., after shear melting in 3D [13] or driven by electric fields [14]), but it has turned out to be much more difficult to drive the equilibrium melting transition in a manner that permits experimenters to track the process dynamically. Recently, quantitative colloidal studies of melting have been shown to be possible. A critical development in this regard has been the fabrication of temperature-sensitive micrometer sized N-isopropylacrylamide (NIPA) microgel spheres [15, 16]. With these colloidal spheres, melting [5, 10, 15, 17], freezing [18], glass transitions [19] and jamming transitions [20] can be driven by moderate temperature changes in a single sample which tune particle diameter and thus colloid volume fraction. NIPA colloidal crystals have been observed to melt from grain boundaries via a first-order transition in 3D [15], and exhibit a two-step melting process with a middle hexatic phase in 2D [10].

Multilayer colloidal spheres confined between two walls are known to exhibit interesting crystalline structures. Hard spheres confined between two walls exhibit a cascade of phases: $1\triangle - 2\square - 2\triangle - 3\square - 3\triangle - 4\square \cdots$ as the wall separation increases [21–24]. Here $n\triangle$ denotes an $n$-layer triangular lattice, and $n\square$ denotes an $n$-layer square lattice. The detailed phase diagram of hard spheres of less than 6 layers has been produced through Monte Carlo simulations [21, 25]. In our NIPA colloidal crystals, square lattices vanish at about 7 layers and spheres only self-assemble into $n\triangle$ when $n > 7$. Previous experimental work has focused on the static structures of the thin films [22, 23, 26]; very recently we began investigation of the melting behaviors of these thin film structures [5].

In this longer contribution, we report some qualitatively new experimental observations, we derive more experimental results to support the conclusions of ref. [5], and we provide more experimental explanation and historical/theoretical context for the work. New results in the paper include observation of a novel type of heterogeneous melting from dislocations, observation of the dynamics and interactions of liquid "lakes" embedded in crystalline matrix, a clarification of wall effects, investigation of different melting behaviors exhibited by surface and bulk layers, and a reconsideration of 2D melting experiments (in this system and other systems) which demonstrates that heterogeneous melting is not a significant effect (as has been previously speculated). We show again that thin films with $<$ 4-layers melt homogeneously, even for polycrystalline films (correcting incorrect terminologies from Table 1 of ref. [5]). The latter behavior is qualitatively different from melting in 3D colloidal or molecular crystals wherein preemptive heterogeneous melting is always dominant and homogenous melting is suppressed even for samples that are rapidly heated.

The paper is organized as follows. In section II, we describe the experimental method. Sections III-VI are primarily concerned with melting of polycrystalline films. Section III is concerned with thick film ($>$ 4-layer) melting. We describe the dislocation melting mechanism and the dynamics of liquid lakes. In section IV, we review 2D melting experiments in colloidal and granular systems, and we show that grain-boundary melting and interfacial melting simply do not exist in these experiments as has been previously speculated. In Section V, we show that thin-film (2- to 4-layer) melting, like 2D melting, is also a homogenous process, except that no intermediate hexatic or tetratic phases are found. We also compare melting of surface and bulk layers, as well as the effects of rough and smooth walls on melting. Section VI shows that the buckled crystals have the same melting behaviors as the normal crystals, with the same 4-layer critical thickness. Section VII is concerned with single-crystal melting. We show that interfacial melting dominates in single crystals of greater than 30 layers. In section VIII, we discuss the order of the melting phase transition, and in the final section we summarize results and address a few open questions.

## II. MATERIALS AND METHODS

For these experiments, fluorescent (rhodamine) labeled uniform ($<$3% polydispersity) NIPA microgel spheres were synthesized and suspended in an aqueous buffer solution with 1 mM acetic acid. The microgel particles were sterically stabilized; electrostatic repulsions between the weakly charged spheres were negligible in the buffer solution. Particle potentials, $u(r)$, were directly measured from the radial distribution function, $g(r)$, in a dilute (area fraction $\sim$ 10%) monolayer of spheres [27, 28]. A small bright-field image artifact [29] was corrected at each temperature using the method described in ref. [30], so that both bright-field and fluorescent microscopies yielded the same $g(r)$ and $u(r)$. Different batches of NIPA spheres exhibited similar short-ranged and repulsive pair potentials (see, for example of one batch, Fig. 1). We define the effective particle diameter, $\sigma$, from the relation $u(\sigma) = 1k_BT$. For our quantitative experiments (Section V), $\sigma$ varied linearly from 1.27 $\mu$m at 24.1°C to 1.14 $\mu$m at 28.0°C. For more qualitative experiments in the other sections, both this batch and another batch

(∼30% smaller) of NIPA spheres were used, and both batches exhibited the same qualitative melting behaviors. By increasing the temperature, we can decrease the volume fraction and drive the melting transition. Solid-solid transitions were not observed.

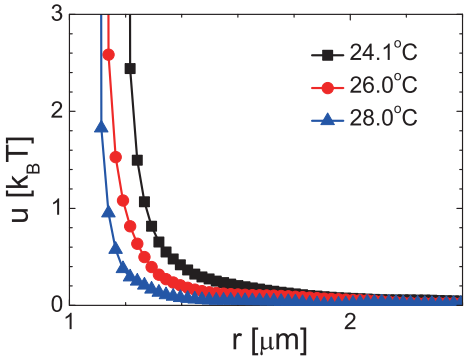


FIG. 1: The pair potentials, $u(r)$, of NIPA spheres at 24.1°C, 26.0°C and 28.0°C.

Thick samples with more than 30 layers were loaded into $18 \times 3 \times H$ mm$^3$ glass channels, where $H$ is the distance between the two parallel rectangular spacers. The flow of the colloidal suspension during loading effectively annealed several layers near the two glass walls into single crystals, while the bulk layers remained glassy. We then increased the temperature close to the melting point so that bulk glassy layers also annealed into a single crystal after 10 hours. Note, imperfect flows and imperfect annealing can readily produce polycrystalline solids (polycrystals). Polycrystals can also be obtained by melting the film and then rapidly recrystallizing it. The domain size within the polycrystalline film can be controlled by varying the crystallization rate.

For thin samples of less than 30 layers, it is not convenient to use spacers, so colloidal suspensions were directly added between the two walls. Flow during loading was thus along all directions in 2D, and the resultant samples formed polycrystals with the domain size ranging from 10 to 500 $\mu$m. Thinner samples had smaller crystalline domains. The sample thickness was roughly controlled by the added volume of colloidal suspension before we sealed the sample and fixed its thickness. For example, a 1.5 $\mu$L colloid usually formed two layers at the center and four layers at the edges of a $1.8 \times 1.8$ cm$^2$ area. Wall bending was small (∼ 1-2 $\mu$m over 1.8 cm); therefore, the local thickness could be taken as uniform over an approximately 100 $\mu$m field of view. The glass surfaces were rigorously cleaned so that particles would not stick to the walls. Surfaces that were not thoroughly cleaned typically acquired a layer of randomly stuck NIPA spheres; these surfaces were used to study the effects of rough-surfaces on melting.

Finite-size effects are important in low-dimensional melting. In 2D, long wavelength critical fluctuations are responsible for the continuous transitions in KTHNY theory. A recent large-scale (with four-million hard disks) simulation showed that 2D melting behavior is different when the system is not sufficiently large [31]. In experiment, however, large crystalline domains are difficult to obtain, especially in the thinner samples. For example, the typical domain size in our two-layer film was only $\sim 10^2$ particles. To circumvent this issue, we applied a mechanical vibration in the vertical direction to samples near the melting point; this procedure introduced a periodic flow inside the sample which effectively annealled the polycrystalline solid so that its domains became much larger, i.e., ∼mm sized domains with $10^6$ particles per layer for which finite-size effects are expected to be negligible [31].

Before the experiment, we used the temperature controller to cycle the temperature slightly below the melting point. This procedure annealled some small defects away and released possible pressure that might have built up during the flow.

The temperature controller (Bioptechs) on the microscope has a resolution of 0.1°C. We increased the sample temperature at a rate of 0.2°C/step. At each temperature, 5 minutes of video were recorded in bright-field microscopy, 2 to 4 minutes of video were recorded for each layer in confocal microscopy, and 1 to 10 3D confocal scans of the static structure were taken. Video rates were 30 frames/sec in bright-field microscopy and 7.5 frames/sec in confocal microscopy [32]. The particle positions in each frame were obtained using standard 2D and 3D image analysis algorithms [33]. Note, the refractive index of NIPA spheres is close to water so that we can see through many layers of crystals even in the bright field [15].

## III. THICK-FILM (> 4 LAYERS) MELTING

### A. Heterogeneous Melting

For 3D crystals, surface melting at the crystal-vapor interface is known to dominate other types of melt nucleation processes [1, 34]. If the crystal is fully enclosed by a solid container, i.e., without a crystal-vapor interface, then it exhibits either grain-boundary melting or interfacial (crystal/solid-wall) melting, depending on which interfacial energy is larger. Polycrystalline NIPA colloidal crystals confined by flat walls are observed to melt only from grain boundaries, i.e., interfacial melting is suppressed [15]. In this contribution, we show that such grain-boundary melting persists in thick films with more than 4 layers [5].

Interestingly, in the present study we have discovered that, when the film is not too thick (i.e. 5- to about 12-layer), melting can start from both dislocations and grain boundaries as shown in Fig. 2. In Fig. 2(a), a grain

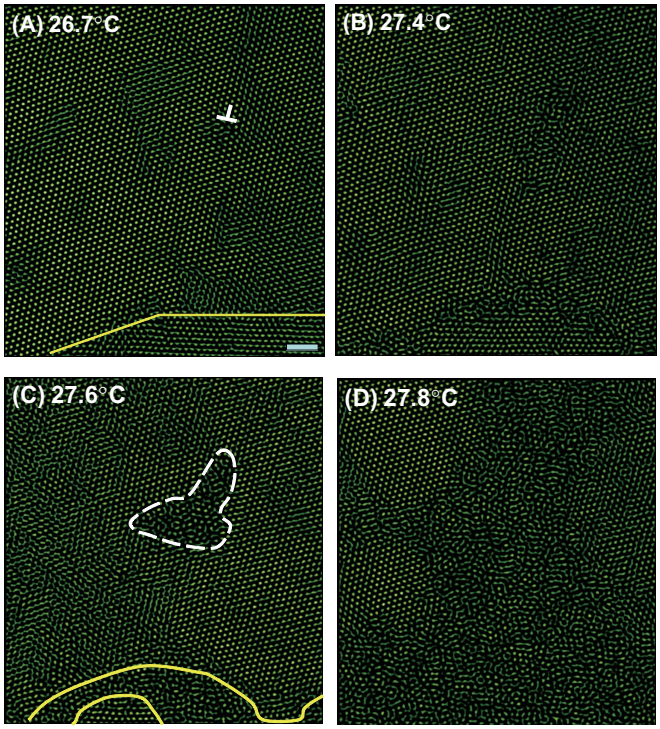


FIG. 2: The heterogeneous melting of a 5△ polycrystalline film. Images are 2D slices taken from the middle of the film. The liquid regions look almost identical in different layers. (a) 26.7°C: The solid line near the bottom of the image highlights the grain boundary and the ⊥ symbol highlights the dislocation. (b) 27.4°C: Liquid began to nucleate at both the grain boundary and the dislocation. (c) 27.6°C: The grain boundary has melted into a liquid strip marked by the two solid lines, and the dislocation has melted into a liquid "lake" marked by the dashed loop. (d) 27.8°C: Liquid grows from lakes and strips of liquid. In equilibrium, the entire crystal melts. Scale bar: 5 $\mu$m.

boundary and a dislocation are marked. As temperature is increased, liquid nucleates at both the grain boundary and the dislocation (Fig. 2(b)), and then forms a cylindrical liquid "lake" embedded in the crystalline domain (Fig. 2(c)). Eventually, this lake grows through the whole sample at an even higher temperature (Fig. 2(d)). The experiments indicate that melting starts simultaneously from every layer, whenever the dislocation has penetrated through the whole film. If the dislocation only exists in a few of the film layers, then the fluid was found to nucleate at the intersection of the dislocation and the glass wall; subsequent invasion of the bulk along the dislocation, and, eventually, a cylindrical liquid lake is formed throughout the film. Although all dislocations do not 'melt' into lakes, all lakes were produced by dislocation melting. Indeed, every lake we observed could be associated with a nonzero Burgers vector (see Fig. 3), and if temperature was decreased, then every lake we observed recrystallized into a dislocation.

Dislocations were observed to melt more easily in thinner films and in larger crystalline domains at higher heating rates. For example, 12-layer films do not melt from dislocations unless the heating rate is very high ($\sim$ 0.1°C/sec), while 7-layer films with domains of $>$ 100 $\mu$m always exhibit dislocation melting, even if the temperature was changed by only 0.1°C every 30 minutes. Hence, when the polycrystalline films are as thin as 5-7 layers with domains of more than 100 $\mu$m, then the energy difference between the grain-boundary melting and the dislocation melting becomes comparable to the thermal energy and lakes can always be generated. The lakes have irregular shapes without obvious facets, suggesting low surface tension in all lattice directions. Multiple lakes can be generated within one large crystalline domain (see Movie 1 in the Supporting Materials). The Burgers vectors of two neighboring lakes in $n\triangle$ crystals are usually oriented differently by an angle of $\pi/3$, occasionally $\pi/2$; they are never antiparallel, because such dislocations readily annihilate before lakes are formed, especially when the crystal is close to the melting point.

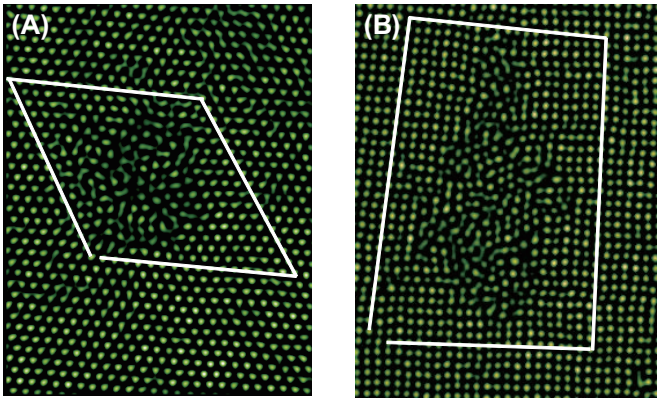


FIG. 3: (a) A liquid lake in a 7△ film. (b) A liquid lake in a 5□ film. The Burgers circuits around the lakes indicate that the two liquid regions have nonzero Burgers vectors, and thus suggest that they were melted from dislocations. Images are 2D slices taken from the middle of the film. Liquid regions look roughly the same in all layers.

### B. Lake Dynamics

Lakes exhibit complex dynamics that are different from the motions of dislocations. Dislocations mainly move along the Burgers vector (i.e., gliding), and occasionally move perpendicular to the Burgers vector (i.e., climbing) [4]. Dislocation gliding involves no change in particle number and hence can proceed rapidly, e.g., moving 1 lattice constant per 5 sec in our samples. In contrast, the diffusion of an isolated lake is much slower, more random and independent of the direction of its Burgers vector. When a lake is situated within 10 lattice constants of a

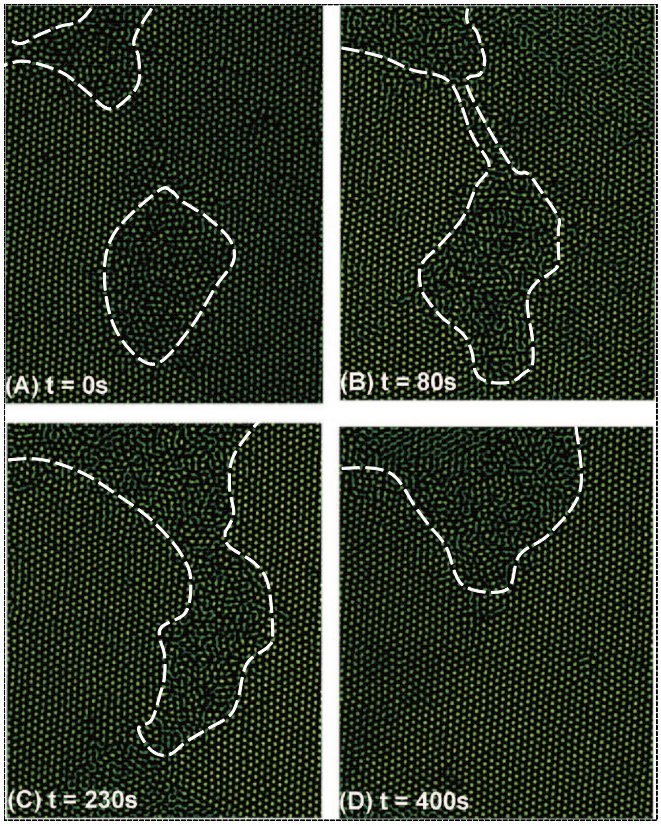


FIG. 4: Two liquid regions gradually merge into one. At (a) 0 s; (b) 80 s; (c) 230 s; and (d) 400 s. When the liquid regions are within about 10 lattice constants of each other, the crystalline region between them can easily melt into a liquid tunnel, as shown in (b). The dashed lines mark the liquid-crystal interfaces. These images show the bottom surface layer. Other layers have the same liquid regions.

grain-boundary-induced liquid strip, the two will deform towards each other (see the liquid strip in the upper left corner and the lake in the center of Fig. 4(a)). Eighty seconds later, a liquid channel was formed between the lake and the liquid strip as shown in Fig. 4(b). Ultimately, the liquid channel became wider and the two liquid domains became closer in order to minimize crystal-liquid interfacial energy (see Fig. 4(c)). After several minutes, the lake irreversibly merged with the liquid strip as shown in Fig. 4(d). Finally the liquid area transformed back into a smooth strip due to the surface tension at the solid-liquid interface. The attraction between a lake and a strip is stronger for larger lakes and at smaller separation distances. Similar merging behaviors exist between two lakes. The heating rate during the formation of the lakes affects their mobilities and stabilities. Rapid heating results in more lakes with more energetic drifts. At times, the drift speed was so high ($\sim 2$ $\mu$m/sec) that the lake became elongated or even dumbbell-shaped, while the area of the lake was roughly preserved. Slow heating produces in fewer lakes with very slow diffusions.

To the best of our knowledge, the heterogeneous melting from dislocations and the resulting lakes have not been reported in other experiments and simulations. Note, this *heterogeneous* melting is different from the conventional dislocation-mediated melting scenario [1, 35, 36] in *homogeneous* melting. Dislocation-mediated melting theory describes a homogeneous scenario wherein more and more dislocations are excited in the perfect crystal as the temperature increases, which, in turn, further lowers the creation energy for additional dislocations. When the creation energy is sufficiently small, an avalanche of dislocations is produced at the melting transition. The mobility of a dense array of dislocations results in sample fluidity [1]. This dislocation-mediated melting scenario, adopted in 2D melting theories [1, 2], is qualitatively different from our observations of dislocation melting in 5- to 12-layer films.

### C. The Equilibrium Phase

The equilibration times of our NIPA samples ranged from a few minutes to several hours. Faster heating rates and thinner films required longer equilibration times. For 5- to 12-layer films with liquid lakes, it often took a few hours for the lakes to diffuse and merge irreversibly into strips. The final equilibrium state is the coexistence of large crystalline domains and large strips of liquid. The liquid-solid coexistence regime in the 300-layer sample is about 6% in volume fraction [5], which is close to the 5% coexistence regime (from 54.5% to 49.5%) in the well-known 3D hard sphere phase diagram [37]. In ref. [5], we showed that the liquid-solid coexistence regime decreases with the film thickness and vanishes completely at 4 layers.

## IV. 2D MELTING

Speculations about 2D crystals have led to similar ideas about edge melting (i.e., the 2D analogy of surface melting), grain-boundary melting and interfacial melting as in 3D crystals [1]. Evidence for edge melting at crystal-vapor interfaces was observed in submonolayer molecular films [38], but, to our knowledge, 2D grain-boundary melting and interfacial melting have not been reported.

Here we review the previous 2D colloidal melting experiments in the literature [8–12, 39] and show that grain-boundary melting and interfacial melting did not occur in those experiments. In fact, those experiments focused on testing 2D melting theories [3, 4, 40, 41] rather than on searching for grain-boundary melting and interfacial melting.

Note that both KTHNY [3, 4] and the grain-boundary [40] melting scenarios describe dislocation-mediated melting [1] in single crystals. According to

KTHNY theory [3, 4], the thermally excited dislocations are well dispersed and preserve the quasi-long-ranged orientational order in the hexatic phase; while grain-boundary melting theory [40] predicts that dislocations condense into grain boundaries when the core energy of the dislocation is lower than a critical value. These grain boundaries disrupt orientational order and preempt the hexatic phase. These theories can be conveniently studied in simulations of 2D single crystals with periodic boundary conditions, but real 2D crystals usually have edges and grain boundaries. To test the 2D melting theories, most experiments have approximated the central area of a large polycrystalline film domain as a single crystal [8–10]. True 2D single crystals have been produced by $10^5$ magnetic colloidal spheres via magnetic-field annealing (with some dislocations but no grain boundaries) [11] and $\sim$ 600 millimeter-sized steel balls achieved through Coulomb repulsion [39]. At high densities, these particles can form single crystals due to the confinement of the container boundaries. Suppose 2D melting is heterogeneous, then liquid should nucleate at grain boundaries in polycrystalline samples (i.e., as in ref. [8–10]) and at container boundaries in single crystals (i.e., as in ref. [11, 39]), and then the liquid should propagate into crystalline domains and sweep across the field-of-view along one direction. Such heterogeneous melting in 2D has never been reported in experiment or simulation. Evidently, grain boundaries and container boundaries do not form liquid domains and suppress homogenous melting in the bulk. This qualitative difference between 2D (homogeneous) and 3D (heterogeneous) melting can be clearly observed in Movie 2 and Movie 3 in the Supporting Materials of the present paper. In fact, if 2D crystals melt heterogeneously, they [8–11] should not be used for testing 2D melting theories [3, 4, 40, 41], which assume homogeneous melting of a single crystal.

Apart from their different melting processes, 2D and 3D melting have different phase behaviors at equilibrium. The intermediate hexatic phase was observed in many 2D systems including our NIPA monolayers [10], while the liquid-solid coexistence without a hexatic phase [42, 43] and the hexatic-liquid coexistence [44] were observed in other systems. In these coexistence states, or in the uniform hexatic phase, small defects are dispersed uniformly without condensing into large strips of liquid or lakes. This behavior is qualitatively different from the liquid-solid coexistence in 3D melting.

## V. THIN-FILM (2-4 LAYERS) MELTING

### A. Homogenous Melting in the XY-plane

In contrast to the heterogeneous melting in thick films, thin films ($\leq$ 4 layers) melt homogeneously from everywhere in the xy-plane (i.e., the transverse plane). This behavior is similar to that observed in 2D melting. Figure 5 shows typical particle trajectories in the 2$\triangle$ phase and the 3$\square$ phase as a function of temperature. Notice, a slight increase in the sample temperature by 0.2°C causes whole crystalline structures to break down from within the domains. At the melting point, many defects and string-like motions were generated (see Fig. 6). Disordered particles form small unstable defect clusters, but they never nucleate into large stable liquid domains such as lakes or strips (see Movies 1-3 in the Supporting Materials). This distinguishes 2- to 4-layer thin film melting from typical 3D homogenous melting in which the liquid nucleus is generated at random sites, and then it rapidly grows once the nucleus exceeds a critical size. Once the critical nucleus is formed, it will dominate the melting dynamics. We did not observe an obvious critical nucleus in our thin films, since large nucleus easily and often breaks into smaller parts.

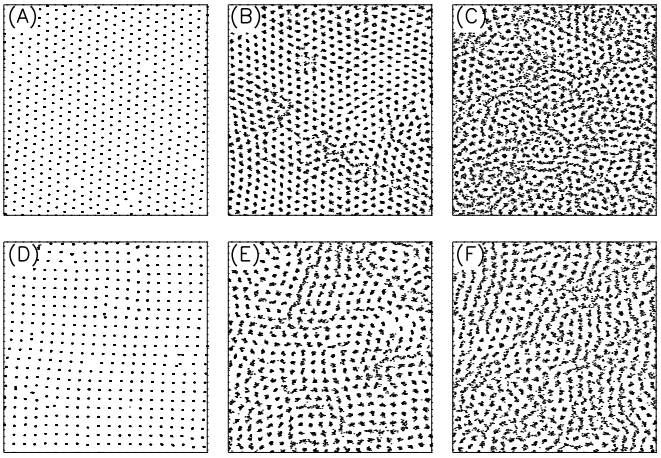


FIG. 5: Typical 10-sec trajectories of the homogenous melting in 2$\triangle$ (a-c) and 3$\square$ (d-f). Each figure is a subarea of a surface layer. (a) In the solid phase at 26.6°C; (b) At the melting point of 28.6°C; (c) In the liquid phase at 28.8°C; (d) In the solid phase at 26.0°C; (e) At the melting point of 27.9°C; (f) In the liquid phase at 28.1°C.

Liquid thin films contain small crystalline patches in equilibrium (see Figs. 5(c,f)). Note, however, such patches do not unambiguously imply a solid-liquid coexistence because patches can also arise in dense fluid phases [10, 45, 46]. Indeed, we observed that small crystalline patches and liquids are not stable and constantly exchange particles. This behavior is different from the coexistence of very large and stable crystalline domains and strips of liquid. Perhaps, the thinner films are more vulnerable to long wavelength density fluctuations [2], and, below 4 layers, thermal fluctuations become strong enough to break up large crystalline domains into small patches and prevent small defects from condensing into large liquid domains. These behaviors have also been observed in 2D melting experiments and simulations.

The homogenous melting of thin films in the xy plane

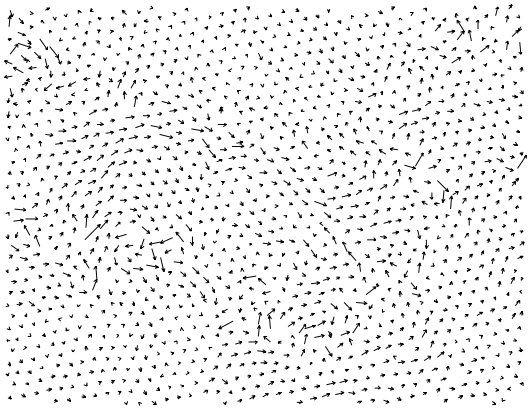

FIG. 6: The 10-sec displacements of the surface layer in a 3△ sample exhibit string-like motions at the melting point of 28.0°C.

enables us to measure the structures and dynamics without concern about melting effects from outside of the field-of-view, e.g. from grain boundaries or edges (see Movie 2 and Movie 3 in the Supporting Materials). Our measurements were carried out on a (60 $\mu$m)$^2$ (∼2300 particles) central area in a large ∼1 mm$^2$ domain obtained through vibration annealing. The vibration method was not very effective for generating large domains of 2□ crystals and some intermediate buckled phases [21], hence we only measured the melting of 2△, 3□, 3△ and 4□ crystals.

### B. 2D and 3D Order Parameters

The density profiles of thin films in the z direction show that the particles stratify into well separated layers, even in the liquid phase near the melting point. Thus we identified the film phases in a layer-by-layer manner at each temperature. Compared with 3D imaging by scanning the z direction with confocal microscopy, the layer-by-layer 2D imaging has better spatial and temporal resolution, substantially more data giving better statistics, measurable dynamics, and the data afford simpler analyses. As a check, we also measured the 3D order parameters [47] by confocal microscopy and obtained the same melting point as in the 2D analysis.

In the 2D analysis, we first labeled each particle with $\{x_j, y_j, t, \psi_{6j}(\text{or } \psi_{4j}), \psi_{Tj}\}$ [4, 10]. Here $t$ is time,

$$\psi_{6j} = \frac{1}{nn_j} \sum_{k=1}^{nn_j} e^{6i\theta_{jk}} \tag{1}$$

or

$$\psi_{4j} = \frac{1}{nn_j} \sum_{k=1}^{nn_j} e^{4i\theta_{jk}} \tag{2}$$

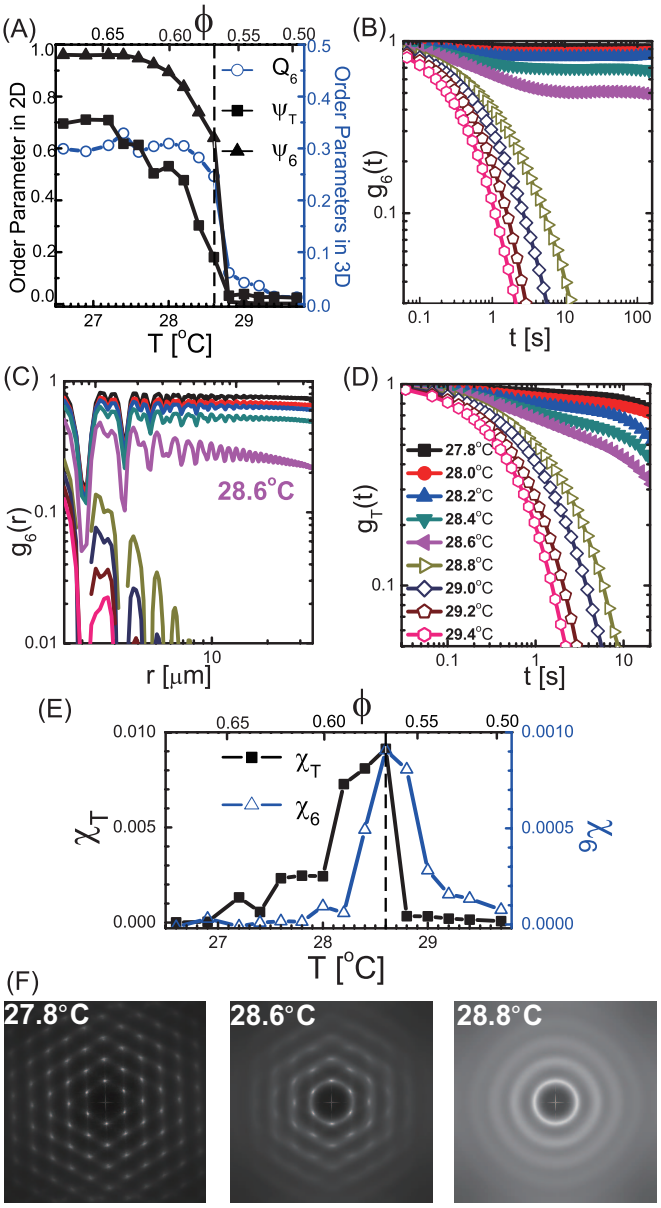


FIG. 7: The melting of a 2△ crystal measured from one of the two surface layers. (a) The 2D translational, 2D and 3D orientational order parameters, $\psi_T$, $\psi_6$ and $Q_6$, respectively, as a function of sample temperature $T$ and packing fraction $\phi$. The vertical dashed line indicates the estimated melting temperature of 28.7°C. (b) Orientational correlation functions $g_6(t)$ in time. Open symbols: liquid phase. Solid symbols: solid phase. (c) Orientational correlation functions $g_6(r)$ in space. (d) Translational correlation functions $g_T(t)$ in time. Open symbols: liquid phase. Solid symbols: solid phase. (e) Translational susceptibility $\chi_T$ and orientational susceptibility $\chi_6$. The vertical dashed line indicates the estimated melting temperature of 28.7°C. (f) Structure factors, $s(k)$, in the solid phase, at the melting point and in the liquid phase. (Note, (a-c,e) have been reported in our previous paper [5]; we include them here to keep the presentation coherent.)

is the bond orientational order parameter for 6-fold (or 4-fold) symmetry, and

$$\psi_{Tj} = e^{i\mathbf{G}\cdot\mathbf{r}_j} \tag{3}$$

is the translational order parameter for particle $j$ at position $\mathbf{r}_j = (x_j, y_j)$. $\theta_{jk}$ is the angle of the bond between particle $j$ and its neighbor $k$. $nn_j$ is the number of nearest neighbors of particle $j$. For triangular lattices, the nearest neighbors can be unambiguously identified by Delaunay triangulation (average number of particle neighbors is 6). For square lattices, the average number of neighbors should be 4. Hence nearest neighbors are further constrained to be those particles within a distance of less than $1.2a$, which is the midpoint between the lattice constant $a$ and the second nearest-neighbor distance $\sqrt{2}a$. $a$ is measured from the first peak position of the radial distribution function $g(r)$. The translational order parameter, $\psi_{_T}$, is sensitive to the primary reciprocal lattice vector $\mathbf{G}$. We first estimated $\mathbf{G}$ from the peak of structure factor $s(k)$, then iteratively varied $\mathbf{G}$ around the initial estimate to maximize $\psi_{_T}$ at each temperature in order to assign an accurate $\mathbf{G}$ [10]. We use the $\mathbf{G}$ of the crystal phase as the initial estimate of $\mathbf{G}$ of the liquid phase [10]. The global order parameter is the averaged order parameter over all $N$ particles:

$$\psi_\alpha = \frac{1}{N}\sum_{j=1}^{N}\psi_{\alpha j} \tag{4}$$

where $\alpha = 6$ (or 4), $T$. $\psi_\alpha$ is 1 for a perfect lattice and is 0 for a totally disordered liquid. Figure 7(a) shows the global $\psi_{_T}$ and $\psi_6$. In the melting of a $2\triangle$ film. The jumps of the order parameters show that the melting point is about 28.7°C.

The 3D orientational order parameter $Q_6$ [47] is also shown in Fig. 7(a). First we defined the neighbors of a particle $i$ as the particles that are within a given radius $r_q$ from $i$ [13]. The $r_q$ is chosen to be the minimum between the first and the second peaks of the measured radial distribution function $g(r)$ [13]. The orientation of particle $i$ to its neighbor $j$ is specified by the unit vector $\hat{\mathbf{r}}_{ij}$. The global orientational order parameter [48]

$$\bar{Q}_{lm} \equiv \langle Y_{lm}(\hat{\mathbf{r}}_{ij})\rangle, \tag{5}$$

where $\langle\ \rangle$ is the ensemble average over all neighbor pairs $(i, j)$. $\bar{Q}_{lm}$ depends on the choice of reference frame, but it can be used to construct the rotationally invariant combinations

$$Q_l \equiv \left(\frac{4\pi}{2l+1}\sum_{m=-l}^{l} \mid \bar{Q}_{lm} \mid^2\right)^{\frac{1}{2}}. \tag{6}$$

$Q_l$ is independent of the choice of reference frame. We use $Q_6$ as a measure of the crystalline order. This order parameter is large for all crystal structures [48] and small for isotropic liquids. Although our films only have a few layers, the surface effect appeared to be unimportant to $Q_6$. For example, $Q_6 = 0.575$ for a perfect 3D face-centered cubic (FCC) lattice [48], and is 0.595 for a perfect 2-layer triangular lattice. Nevertheless, it is the jump of $Q_6$, instead of the absolute value of $Q_6$, that reflects the melting transition. In Fig. 7(a), the $Q_6$, $\psi_6$ and $\psi_T$ curves consistently yield the same melting point.

### C. Correlation Functions

Different phases are characterized by the correlation functions of order parameters. The order parameters, $\psi_6$ and $\psi_{_T}$, can be correlated in space or time and yield four correlation functions:

$$g_\alpha(r = |\mathbf{r}_i - \mathbf{r}_j|) = \langle\psi^*_{\alpha i}(r_i)\psi_{\alpha j}(r_j)\rangle, \tag{7a}$$

$$g_\alpha(t) = \langle\psi^*_{\alpha i}(\tau)\psi_{\alpha i}(\tau + t)\rangle, \tag{7b}$$

where $\alpha = 6$ (or 4), $T$.

KTHNY theory predicts that both $g_6(t)$ and $g_6(r)$ approach a constant in a crystal (long-ranged orientational order), decay algebraically in the hexatic phase (quasi-long-ranged orientational order) and decay exponentially in the liquid phase (short-ranged orientational order). From the $g_6(t)$ shown in Fig. 7(b), we can clearly resolve a crystal phase below 28.7°C and a liquid phase above 28.7°C. The hexatic phase characterized by the algebraic decay was not observed. The $g_6(r)$ in Fig. 7(c) exhibit similar behavior to the $g_6(t)$, but the crystal at 28.6°C appears to decay algebraically. We attribute this observation to finite-size effects rather than a signature of the hexatic phase. In fact, the $g_6(t)$ at 28.6°C also exhibits a power-law decay initially, but it becomes constant at longer times.

In KTHNY theory, the translational time correlation functions, $g_T(t)$, decay algebraically in the solid phase (quasi-long-ranged translational order) and exponentially in the hexatic and liquid phases (short-ranged translational order). Fig. 7(d) shows that the $g_T(t)$ of $2\triangle$ decays algebraically below 28.7°C and exponentially above 28.7°C, which is consistent with the measured melting point.

### D. Susceptibilities

Another signature of a phase transition is the divergence (or discontinuity) of the order-parameter susceptibility $\chi$. This method avoids finite-size or finite-time ambiguity and is more accurate than the methods described in previous subsections B and C [10]. The susceptibility,

$$\chi_\alpha = \lim_{A\to\infty} A\left(\langle|\psi^2_\alpha|\rangle - \langle|\psi_\alpha|\rangle^2\right), \tag{8}$$

is the time fluctuation of the global order parameter in area $A$. We calculated $\chi$ for sub-areas of different sizes and extrapolated to the infinite-size limit [10]. Without such extrapolation, the melting point can still be correctly measured, since the position of the divergent peak of $\chi$ remains unchanged as long as the finite-sized area is not too small. However the measurement of $\chi$ requires lots of statistics, or else the results are noisy. In Fig. 7(e), both $\chi_T$ and $\chi_6$ peak at the same point, which indicates a one-step transition without a middle phase. In contrast, $\chi_T$ and $\chi_6$ of a NIPA monolayer (i.e., a 2D system) diverge at different temperatures [10], which signals the presence of an intermediate hexatic phase.

### E. 3- and 4-layer Films

Subsections B-D referred to the 2△ film. 3□ and 3△ films have similar order parameters, correlation functions and susceptibilities (see Figs. 8, 9). The results for 4□ are also similar but are more noisy due to limited statistics and more defects in the square lattices.

In 3□ and 3△ films, the translational and orientational susceptibilities peak at the same point (i.e., same temperature/packing-fraction), indicating one-step melting transitions (see Fig. 8(e) and Fig. 9(e)). Corresponding order parameters and the correlations in Fig. 8(a-d) and Fig. 9(a-d) also yield the same melting points. Note that the transition volume fraction can correspond to different temperatures in different samples, because the initial volume fractions in the sample preparation are slightly different.

If we assume that the susceptibilities are symmetric around the peak, the divergent peak can be further interpolated to 0.1°C resolution. For example in Fig. 8(e), the data points at 28.2°C and 27.8°C are slightly asymmetric to 28.0°C. Hence the exact transition temperature is within 28.0-28.2°C and 28.0°C belongs to the solid phase as shown in Fig. 8(f). In contrast, Fig. 9(f) suggests that 3□ belongs to the liquid phase at 27.9°C. This is consistent with the asymmetry of the $\chi_4$ curve in Fig. 9(e). Moreover, the steepest jumps of the order parameters in Fig. 8(a) and Fig. 9(a) also suggest that the melting temperatures are at $28.1 \pm 0.1$°C for 3△ and $27.8 \pm 0.1$°C for 3□. Hence all measurements yield consistent melting points with 0.1°C resolution.

In square lattices, the melting transition appears to be less sharp than that of the triangular lattices. For example, the order parameter in Fig. 9(a) decreases gradually and the correlation functions in Fig. 9(b) do not exhibit a clear boundary between crystal and liquid phases. We also observed that square lattices have more defects and noise compared to the triangular lattices. This observation is consistent with the fact that the (111) plane of the FCC hard-sphere crystal wets the flat surface best [49]. Note that multilayer triangular lattices are FCC crystals with the (111) plane along the walls, and multilayer square lattices are FCC crystals with the (100) plane along the walls.

### F. Surface Layers versus Bulk Layers

The above 2D analyses in subsections B-E are based on the behavior of surface layers next to the walls. It is natural to inquire about whether the behavior of all layers in the thin film are the same. We found that bulk layers and surface layers melt at the same temperature (see Fig. 10 and Fig.11). For example, all the order parameters, correlation functions and susceptibilities in Fig. 10 show that the melting temperature of 3□ is 27.9°C for both the surface and the bulk layers. For 3△, all the results in Fig. 11 show that both the bulk and the surface layers melt at 28.0°C, although $\chi_6$ of the bulk layer peaks at 28.2°C. We attribute this difference of 0.2°C to experimental error because the temperature controller has 0.1°C resolution and the temperature is changed at 0.2°C/step. In fact, Figs. 11(a-c) show that the exact transition point is between 28.0°C and 28.2°C.

Near the melting point, $g_4(t)$ or $g_6(t)$ of the surface layer decay faster than the corresponding correlation functions of the bulk layers (see Figs. 10(a,b) and 11(a,b)). This difference in behavior is apparent in the videos which showed that surface layers disorder more rapidly than bulk layers. Hence the surface and the bulk layers have the same equilibrium phase, but their kinetic paths toward equilibrium proceed at different rates.

Thin films ($\leq$ 4 layers) clearly exhibit homogenous melting in the xy plane. For mono- and 2-layer films, the melting must be homogenous in the z direction because there are no bulk layers. For 3- and 4-layer films, both surface layers and bulk layers appeared to melt simultaneously, at least within our spatial, temporal and temperature resolutions, but they evolve towards their final equilibrium states at different rates. This observations indicates that the melting in the z direction is almost, but not perfectly homogenous.

We further explored the boundary roughness effect on melting. If the glass walls are not rigorously cleaned, or the NIPA colloids are not freshly dispersed, then NIPA spheres will randomly stick to the glass walls and effectively provide a 'roughness' boundary condition. We observed that such rough walls do not affect the melting behavior and the 4-layer critical thickness remains the same as that of the sample confined by flat walls.

## VI. MELTING OF BUCKLED CRYSTALS

When the wall separation cannot be exactly fit by either $n$△ or $(n+1)$□, close-packed spheres will form intermediate buckled phases or prism phases [21, 25, 26, 50].

We observed buckled phases in films of less than ∼10-layers (see Fig. 12). For films of 4-layers or less, the buckled phases occurred in small domains, with each buckled region containing even smaller martensitic stripe domains. Such buckled thin films first appeared to form un-buckled crystals (i.e., normal crystals) upon decreasing the volume fraction, and then these normal crystals melted into the fluid phase upon further lowering of the volume fraction. By contrast buckled crystals of 5- to 8-layers remain buckled, even in the solid/liquid coexistence regime (see Fig. 12), an effect we found somewhat surprising. The melting behaviors (i.e., melting pathways) were basically the same for buckled and normal thin-film crystals (e.g., melting from grain boundaries and dislocations as shown in Fig. 12 in thick films and from everywhere in thin films).

## VII. SINGLE-CRYSTAL MELTING

3D (∼ 300 layers) NIPA colloidal polycrystals confined between flat walls have been demonstrated to melt from grain boundaries [15]. Where does melting start if we employ a single crystal without grain boundaries? This question was raised in ref. [51]. Here we address this question. To this end we fabricated cm-sized single-crystal films with more than 30 layers as described in section II. The single crystals only melted from the film-wall interfaces, and then the liquid phases progress through the bulk. Melting from other defects appears to be completely suppressed by this interfacial melting.

It is similarly interesting to consider whether interfacial melting can suppress dislocation melting in thinner films. For 5- to ∼12-layer polycrystalline films, we have found that dislocation melting can coexist with the grain-boundary melting, and that interfacial melting is suppressed in this regime. Hence nature's preference for the three types of heterogeneous melting might be ordered as follows: grain-boundary melting $>$ or $\simeq$ dislocation melting $>$ interfacial melting in 5- to 12-layer films. Consequently, dislocation melting might be able to dominate and suppress the interfacial melting in 5- to 12-layer single crystals. Note, a single crystal can contain defects such as vacancies and dislocations, but not grain boundaries. Since $>$ 30-layer single-crystal films are dominated by interfacial melting, another 'critical thickness' might be expected between 12 and 30 layers. Dislocation melting dominates below this critical thickness, while interfacial melting dominates above the critical thickness. This critical thickness could be explored experimentally, if single-crystal films thinner than 30-layers could be fabricated.

## VIII. ORDER OF THE PHASE TRANSITIONS

The coexistence of two phases is a signature of the first-order phase transition because finite latent heat cannot be instantaneously transferred between the system and the environment. Therefore the melting of thick films is clearly a strong first-order transition. In thin-film melting ($\leq$ 4 layers), we did not observe the coexistence of large solid and liquid domains within our temperature resolution, hence one is tempted to suggest that the transition in this case is either continuous or weakly first-order.

The order of the phase transition can, in principle, be deduced from the shape of the susceptibility curve [52]. If the two curves on the left- and right-hand-side of the peak have the same asymptotic temperature, then the transition is continuous; otherwise, it is first order [52]. In other words, the susceptibilities around the peak are symmetric for a continuous transition but are asymmetric for a first-order transition. Even though we have measured the susceptibilities in this work, however, we cannot unambiguously distinguish between first-order and continuous transitions due to the limited temperature resolution. Future work with finer temperature control near the phase transition could enable us to pinpoint the order of the thin-film melting transitions more precisely.

## IX. DISCUSSION AND SUMMARY

We have studied the melting behaviors in single- and poly-crystalline colloidal films. Thick films ($>$ 4 layers), thin films (2 to 4 layers) and monolayers exhibit different melting behaviors [5]. For thick polycrystalline films of more than 12 layers, grain-boundary melting dominates and suppresses other melting mechanisms, and for films in the 5- to about 12-layer range, the dislocation melting can coexist with the grain-boundary melting. Thin films ($\leq$ 4 layers) appear to melt homogeneously (even polycrystalline films). We reviewed previous particle-based 2D melting experiments and speculated (based on our observations about thin films and on the descriptions of earlier experimental results) that grain-boundary melting and edge melting did not occur. Finally, we observed that single crystals with more than 30 layers exhibit only interfacial melting from film-wall interfaces. All these features were robust across more than 100 samples made from different batches of microgel particles. In addition to corroborating and extending the work in ourprevious paper [5], we note here that some of the terminology used in the present paper were used with slightly different meanings in ref. [5], see note [53].

To our knowledge, heterogeneous melting from dislocations has not been reported before. Such dislocation melting generates liquid lakes fully embedded in crystalline domains, while grain-boundary melting gen-

erates strips of liquid. Over time, liquid lakes and strips move through the sample an merge together irreversibly. Faster heating can generate more lakes in thinner films, and in films as thin as 5 to 7 layers, lakes can spontaneously form even under our slowest heating rate.

Thick, thin and monolayer films exhibit different phase behaviors at equilibrium. In thick films, the solid-liquid coexistence regime decreases with the film thickness, vanishing at a critical thickness of 4 layers [5]. Thin-films (2- to 4-layers) melt in one step without a middle tetratic or hexatic phase; monolayers melt in two steps with an intermediate hexatic phase [10].

Our results raise several new questions. One obvious question concerns why melting is heterogeneous in thick films and becomes homogenous in thin films. We suspect this behavior arises because thinner films are softer and more vulnerable to fluctuations [2], so that the extra long-wavelength fluctuations in low dimensional systems [2] may break the large crystalline domains from the 'inside'. Another related question concerns why the critical film thickness is 5-layers (or 4-layers). Interestingly, this 'magic number 5' appears to exist in other systems. For example, the estimated critical nucleus size in 3D colloid crystallization ranges from 60 to 160 particles [13], as size which is of order $5^3$; the critical size for 2D colloidal crystalline sublimation [54] and nucleation [55] is about $30 \simeq 5^2$; and the typical size of crystalline patches in our dense liquid thin films is also about $5^2$ particles.) It would be interesting to explore whether the critical length scales of 5 particles share the same underlying mechanism.

## ACKNOWLEDGEMENT

This work was supported by the RGC grant 601208 (Y.H.), by the NSF through grant DMR-080488, the MRSEC grant DMR-0520020, and by NASA through grant NAG-2939 (A.G.Y.).

* Electronic address: yilong@ust.hk

[1] J. G. Dash, Rev. Mod. Phys. **71**, 1737 (1999).
[2] K. J. Strandburg, Rev. Mod. Phys. **60**, 161 (1988).
[3] J. M. Kosterlitz and D. J. Thouless, J. Phys. C **6**, 1181 (1973); D. R. Nelson and B. I. Halperin, Phys. Rev. B **19**, 2457 (1979); A. P. Young, Phys. Rev. B **19**, 1855 (1979).
[4] D. R. Nelson, *Defects and Geometry in Condensed Matter Physics* (Cambridge University Press, UK, 2002).
[5] Y. Peng, Z.-R. Wang, A. M. Alsayed, A. G. Yodh, and Y. Han, Phys. Rev. Lett. **104**, 205703 (2010).
[6] D.-M. Zhu and J. G. Dash, Phys. Rev. Lett. **57**, 2959 (1986).
[7] M. S. Pettersen, M. J. Lysek, and D. L. Goodstein, Phys. Rev. B **40**, 4938 (1989).
[8] C. A. Murray and D. H. Van Winkle, Phys. Rev. Lett. **58**, 1200 (1987).
[9] A. H. Marcus and S. A. Rice, Phys. Rev. Lett. **77**, 2577 (1996).
[10] Y. Han, N. Y. Ha, A. M. Alsayed, and A. G. Yodh, Phys. Rev. E **77**, 041406 (2008).
[11] K. Zahn, R. Lenke, and G. Maret, Phys. Rev. Lett. **82**, 2721 (1999).
[12] U. Gasser, C. Eisenmann, G. Maret, and P. Keim, ChemPhysChem, **11**, 963 (2010).
[13] U. Gasser, E. R. Weeks, A. Schofield, P. N. Pusey, and D. A. Weitz, Science **292**, 258 (2001).
[14] A. E. Larsen and D. G. Grier, Nature **385**, 230 (1997); A. Yethiraj and A. van Blaaderen, Nature **421**, 513 (2003).
[15] A. M. Alsayed, M. F. Islam, J. Zhang, P. J. Collings, and A. G. Yodh, Science **309**, 1207 (2005).
[16] R. Pelton, Adv. Colloid Interface Sci. **85**, 1 (2000); H. Senff and W. J. Richtering, J. Chem. Phys. **111**, 1705 (1999); J. D. Debord, S. Eustis, S. B. Debord, M. T. Lofye, and L. A. Lyon, Adv. Mater. **14**, 658 (2002); J. Wu, B. Zhou, and Z. Hu, Phys. Rev. Lett. **90**, 048304 (2003); L. A. Lyon, J. D. Debord, S. B. Debord, C. D. Jones, J. G. McGrath, and M. J. Serpe, J. Phys. Chem. B, **108**, 19099 (2004);
[17] M. A. Lohr, et al., Phys. Rev. E **81**, 040401 (2010).
[18] Z.-R. Wang, A. M. Alsayed, A. G. Yodh, and Y. Han, J. Chem. Phys. **132**, 154501 (2010).
[19] P. Yunker, Z. Zhang, K. B. Aptowicz, and A. G. Yodh, Phys. Rev. Lett. **103**, 11, 115701 (2009); P. Yunker, Z. Zhang, and A. G. Yodh, Phys. Rev. Lett. **104**, 015701 (2010).
[20] Z. Zhang, et al., Nature **459**, 230 (2009).
[21] M. Schmidt and H. Löwen, Phys. Rev. Lett. **76**, 4552 (1996); M. Schmidt and H. Löwen, Phys. Rev. E **55**, 7228 (1997).
[22] P. Pieranski, L. Strzelecki, and B. Pansu, Phys. Rev. Lett. **50**, 900 (1983).
[23] J. A. Weiss, D. W. Oxtoby, D. G. Grier, and C. A. Murray, J. Chem. Phys. **103**, 1180 (1995).
[24] R. Zangi and S. A. Rice, Phys. Rev. E **61**, 660 (2000).
[25] A. Fortini and M. Dijkstra, J. Phys.: Condens. Matter **18**, L371 (2006).
[26] S. Neser, C. Bechinger, P. Leiderer, and T. Palberg, Phys. Rev. Lett. **79**, 2348 (1997); A. B. Fontecha et al., J. Phys.: Condens. Matter **17**, S2779 (2005); D. K. Satapathy, et al. Euro. Phys. Lett. **87**, 34001 (2009).
[27] S. H. Behrens and D. G. Grier, Phys. Rev. E **64**, 050401 (2001).
[28] Y. Han and D. G. Grier, Phys. Rev. Lett. **91**, 038302 (2003).
[29] J. Baumgartl and C. Bechinger, Europhys. Lett. **71**, 487 (2005).
[30] M. Polin, D. G. Grier, and Y. Han, Phys. Rev. E, **76**, 041406 (2007).
[31] C. H. Mak, Phys. Rev. E **73**, 065104(R) (2006).
[32] P. Habdas and E. R. Weeks, Curr. Opin. Colloid Interface Sci. **7**, 196 (2002).
[33] J. C. Crocker and D. G. Grier, J. Colloid Interface Sci. **298** (1996).
[34] J. Frenkel, *Kinetic Theory of Liquids* (Clarendon, Oxford, pp. 425-426, 1946).
[35] H. Kleinert, *Gauge Theory in Condensed Matter, Vol. II.* (World Scientific, Singapore, 1989).
[36] L. Burakovsky, D. L. Preston, and R. R. Silbar, Phys.

Rev. B **61**, 15011 (2000).
[37] P. N. Pusey and W. van Megen, Nature **320**, 340 (1986).
[38] D.-M. Zhu, D. Pengra, and J. G. Dash, Phys. Rev. B **37**, 5586 (1988); H. Shechter, R. Brener, and J. Suzanne, Europhys. Lett. **6**, 163 (1988); H. Shechter, R. Brener, M. Folman, and J. Suzanne, Phys. Rev. B **41**, 2748 (1990).
[39] X. H. Zheng and R. Grieve, Phys. Rev. B **73**, 064205 (2006).
[40] S. T. Chui, Phys. Rev. Lett. **48**, 933 (1982); Phys. Rev. B **28**, 178 (1983); Y. Saito, Phys. Rev. Lett. **48**, 1114 (1982).
[41] M. A. Glaser and N. A. Clark, Adv. Chem. Phys. **83**, 543 (1993).
[42] H. Weber, D. Marx, and K. Binder, Phys. Rev. B **51**, 14636 (1995).
[43] A. Jaster, Phys. Lett. A **330**, 120 (2004).
[44] W. K. Qi, S. M. Qin, X. Y. Zhao, and Y. Chen J. Phys.: Condens. Matter **20**, 245102 (2008).
[45] A. Z. Patashinski, A. C. Mitus, and M. A. Ratner, Phys. Rep. **288**, 409 (1997).
[46] U. Gasser, J. Phys.: Condens. Matter **21**, 203101 (2009).
[47] P. J. Steinhardt, D. R. Nelson, and M. Ronchetti, Phys. Rev. B **28**, 784 (1983).
[48] P. R. ten Wolde, M. J. Ruiz-Montero, and D. Frenkel, J. Chem. Phys. **104**, 9932 (1996).
[49] S. Auer and D. Frenkel, Phys. Rev. Lett. **91**, 015703 (2003).
[50] Y. Han, et al., Nature, **456**, 898 (2008).
[51] P. N. Pusey, Science **309**, 1198 (2005).
[52] K. Binder, Rep. Prog. Phys. **50**, 783 (1987).
[53] In Table 1 of ref. [5], the terms "grain-boundary melting" and "interfacial melting" do not imply suppression of homogenous melting within crystalline domains. In the present paper, however, we use "grain-boundary melting" (and "interfacial melting") only for heterogeneous melting in thick films wherein liquids nucleate at grain boundaries (or interfaces) and then spread through the bulk, rather than melting from within crystalline domains.
[54] J. R. Savage, D. W. Blair, A. J. Levine, R. A. Guyer, and A. D. Dinsmore, Science **314**, 795 (2006).
[55] J. R. Savage and A. D. Dinsmore, Phys. Rev. Lett. **102**, 198302 (2009).

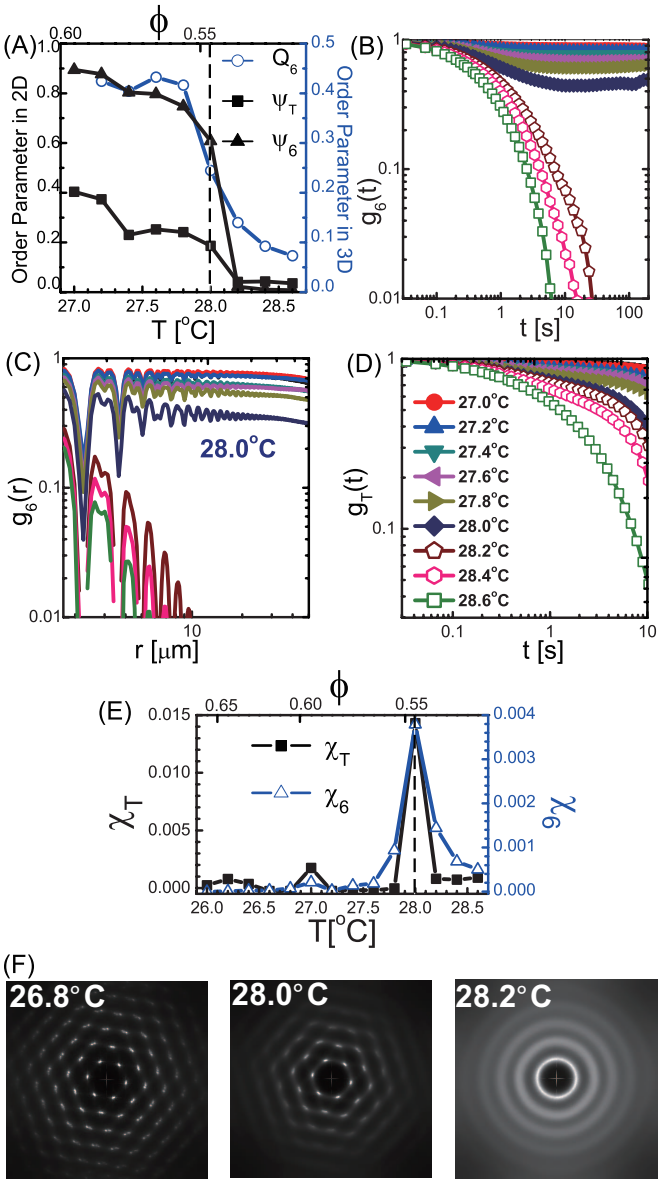


FIG. 8: The melting of a 3△ crystal measured from one of the two surface layers. (a) The 2D translational, 2D and 3D orientational order parameters, $\psi_T$, $\psi_6$ and $Q_6$, respectively, as a function of sample temperature $T$ and packing fraction $\phi$. The vertical dashed line marks the melting point. (b) Orientational correlation functions $g_6(t)$ in time. Open symbols: liquid phase. Solid symbols: solid phase. (c) Orientational correlation functions $g_6(r)$ in space. (d) Translational correlation functions $g_T(t)$ in time. Open symbols: liquid phase. Solid symbols: solid phase. (e) Translational susceptibility $\chi_T$ and orientational susceptibility $\chi_6$. The vertical dashed line marks the melting point. (f) Structure factors, $s(k)$, in the solid phase, at the melting point and in the liquid phase.

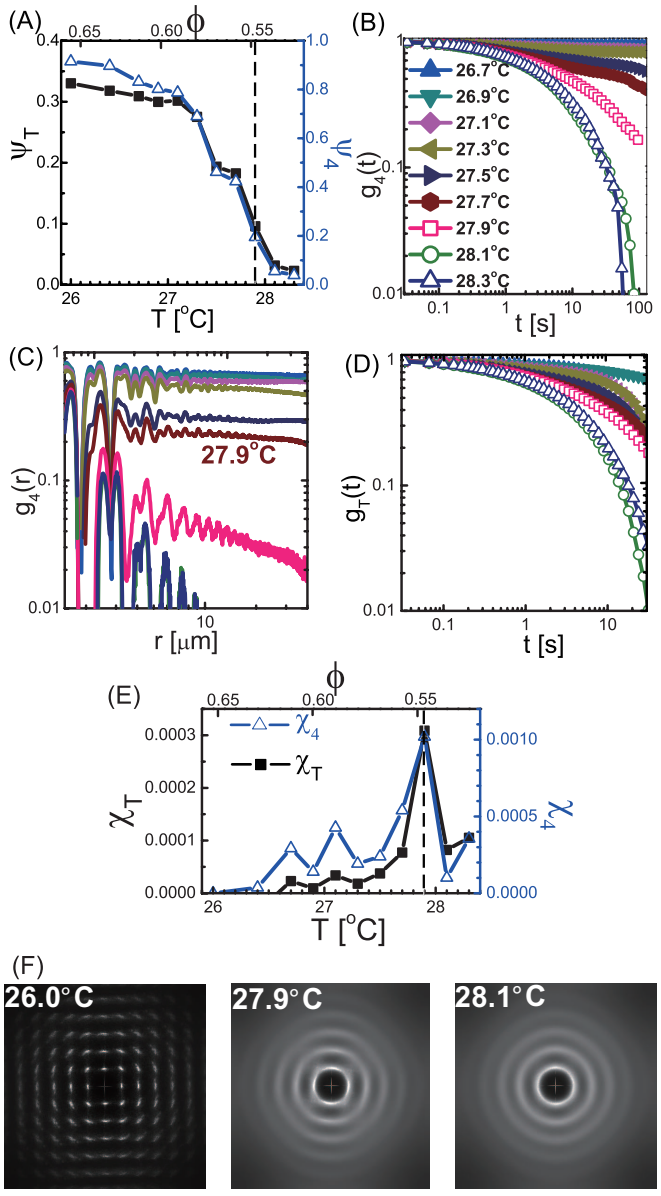


FIG. 9: The melting of a 3□ crystal measured from one of the two surface layers. (a) The 2D translational, 2D and 3D orientational order parameters: $\psi_T$, $\psi_6$ and $Q_6$, respectively, as a function of sample temperature $T$ and packing fraction $\phi$. The vertical dashed line marks the melting point. (b) Orientational correlation functions $g_4(t)$ in time. Open symbols: liquid phase. Solid symbols: solid phase. (c) Orientational correlation functions $g_4(r)$ in space. (d) Translational correlation functions $g_T(t)$ in time. Open symbols: liquid phase. Solid symbols: solid phase. (e) Translational susceptibility $\chi_T$ and orientational susceptibility $\chi_6$. The vertical dashed line marks the melting point. (e) Structure factors, $s(k)$, in the solid phase, at the melting point and in the liquid phase.

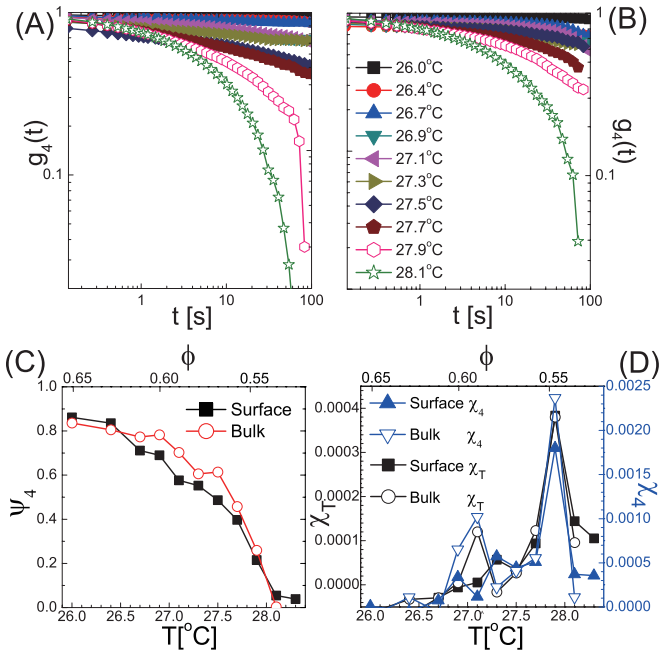


FIG. 10: The surface layers versus the bulk layers in the 3□ sample. (a) Orientational time correlation function, $g_6(t)$, of one of the surface layers. Open symbols: liquid phase. Solid symbols: solid phase. (b) $g_6(t)$ of the bulk layer. (c) Orientational order parameter, $\psi_6$, of the surface layer (open circles) and the bulk layer (solid squares). (d) Translational susceptibility $\chi_T$ and orientational susceptibility $\chi_6$ of the surface layer and the bulk layer.

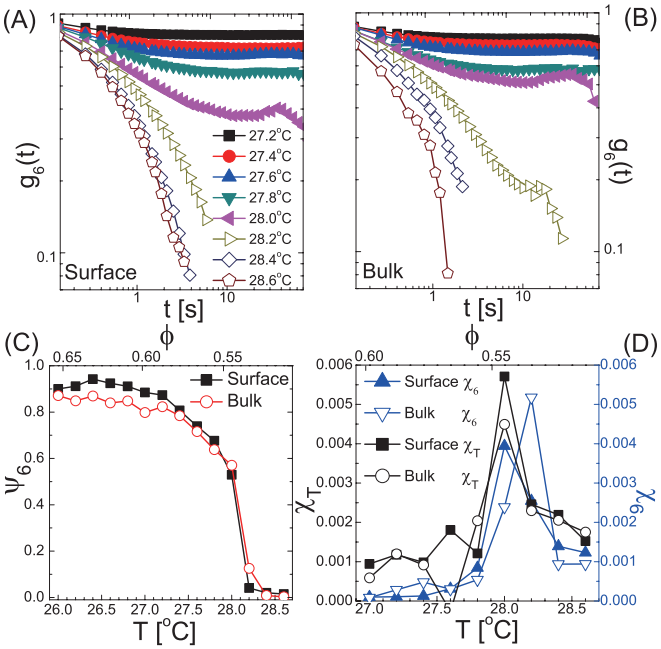


FIG. 11: The surface layers versus the bulk layers in the 3△ sample. (a) Orientational time correlation function, $g_6(t)$, of one of the surface layers. Open symbols: liquid phase. Solid symbols: solid phase. (b) $g_6(t)$ of the bulk layer. (c) Orientational order parameter, $\psi_6$, of the surface layer (open circles) and the bulk layer (solid squares). (d) Translational susceptibility $\chi_T$ and orientational susceptibility $\chi_6$ of the surface layer and the bulk layer.

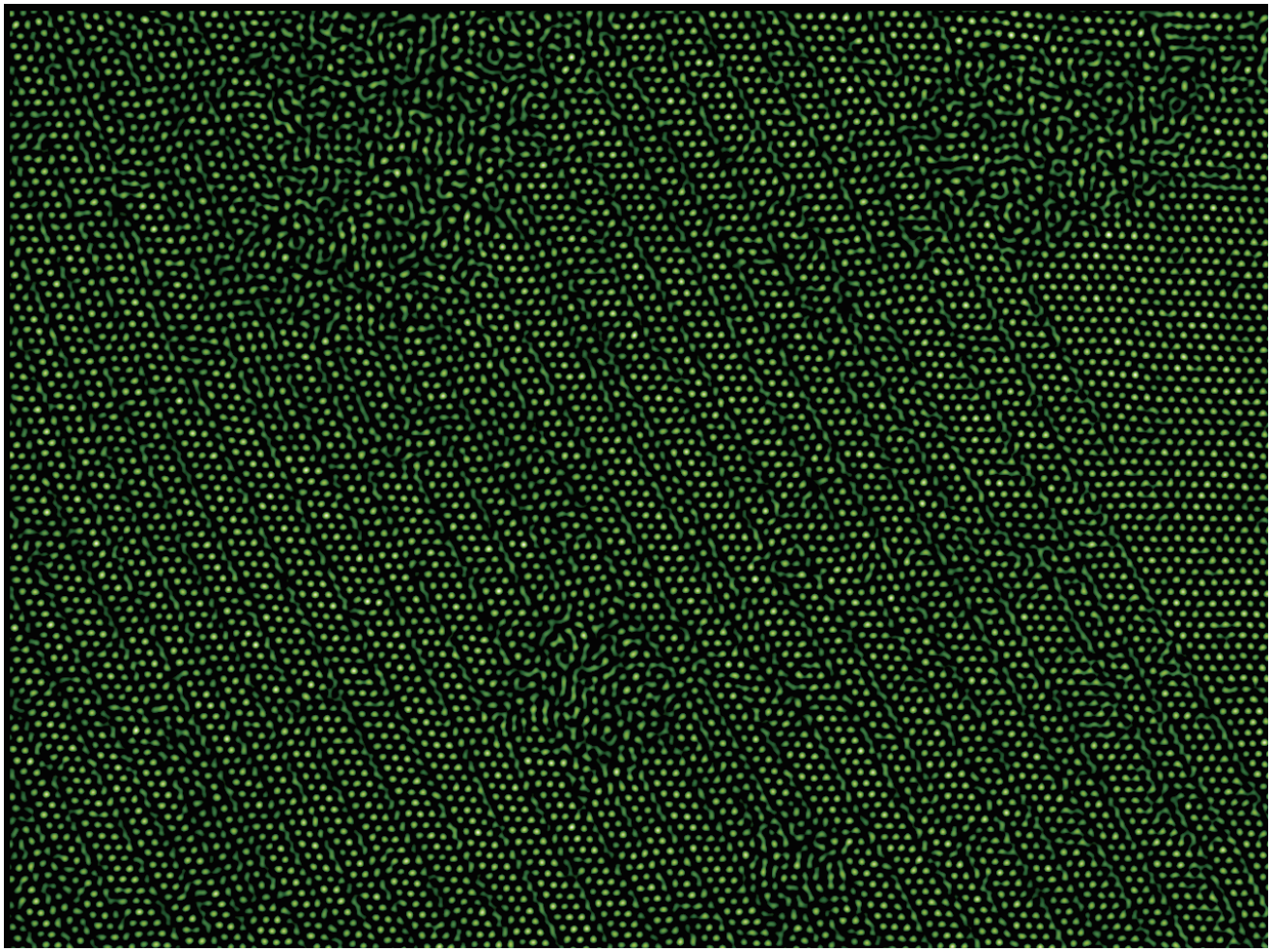

FIG. 12: Lakes in the 8-layer buckled crystalline film. The parallel stripes reflect the buckling. The upper left corner without stripes is normal crystal. The buckling remains in the solid/liquid coexistence regime. Again, images are a 2D slices from the middle of the film. Liquid regions look about the same in all layers.